

Identification of the Nanogold Particle-Induced Endoplasmic Reticulum Stress by Omic Techniques and Systems Biology Analysis

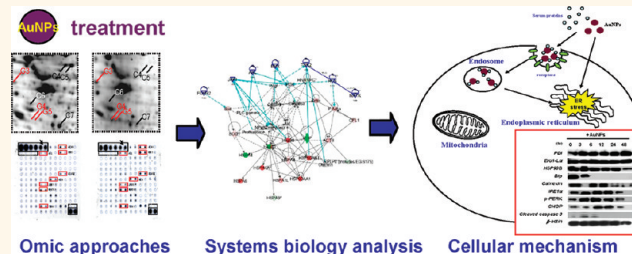
Yen-Yin Tsai,^{†,¶} Yi-Huei Huang,^{‡,¶} Ya-Li Chao,^{†,¶} Kuang-Yu Hu,^{§,#} Li-Te Chin,^{⊥,#} Shiu-Huey Chou,[†] Ai-Ling Hour,[†] Yeong-Der Yao,^{||} Chi-Shun Tu,^{||} Yao-Jen Liang,[†] Cheng-Yuh Tsai,[‡] Hao-Yu Wu,[‡] Shan-Wen Tan,[‡] and Han-Min Chen^{†,||,*}

[†]Department of Life-Science, Fu-Jen Catholic University, Taipei, Taiwan, [‡]Gold Nanotech, Inc., Taipei, Taiwan, [§]Graduate Institute of Medical Sciences, National Defense Medical Center, Taipei, Taiwan, [⊥]Department of Microbiology and Immunology, National Chiayi University, Chiayi, Taiwan, and ^{||}Graduate Institute of Applied Science and Engineering, Fu-Jen Catholic University, Taipei, Taiwan ^{*Y.Y.T., Y.H.H., and Y.L.C. contributed equally to this work. #K.Y.H. and L.T.C. contributed equally to this work.}

Unique electronic, biocompatible, and molecular-recognition properties of small sized nanogold particles (AuNPs) make them easy for biomolecule conjugation.^{1–3} Due to the long history of gold-based compounds used for therapeutic purposes, such as rheumatoid arthritis, cancer, AIDS, bronchial asthma, and malaria,⁴ AuNPs are considered biocompatible and deemed as attractive therapeutic platforms.^{5,6} AuNPs conjugated with vascular endothelial growth factor have been shown to exert antiangiogenic activities against macrophage infiltration and subsequent inflammation.⁷ Moreover, AuNPs have been explored with a great deal of interest as effective and promising agents of cancer chemotherapy.^{5,8} Use of AuNPs had been demonstrated to reduce the systemic toxicity in the tumor necrosis factor (TNF)-mediated antitumor treatment.⁹ Owing to the unique and tunable surface plasmon resonance properties, AuNPs are also well-suited for applications in photothermal cancer therapy.^{10,11}

Since there is considerable potential use in nanomedicines, the cytotoxicity as well as the elicited cellular mechanism by AuNPs has to be evaluated with extreme care. The cytotoxicity of AuNPs has been widely investigated and extensively reviewed. The cytotoxicity of the chemically synthesized AuNPs is considered to be attributed to particle size and surface-modified ligands; that is, smaller AuNPs generally comprise a higher cytotoxicity, and AuNPs conjugated with cationic ligands, such as cetyltrimethylammonium bromide (CTAB), are more toxic to cells than those conjugated with biotin, cysteine, citrate, glucose, and PEG.^{6,12,13} Recently, the

ABSTRACT



Growth inhibition and apoptotic/necrotic phenotype was observed in nanogold particle (AuNP)-treated human chronic myelogenous leukemia cells. To elucidate the underlying cellular mechanisms, proteomic techniques including two-dimensional electrophoresis/mass spectrometry and protein microarrays were utilized to study the differentially expressed proteome and phosphoproteome, respectively. Systems biology analysis of the proteomic data revealed that unfolded protein-associated endoplasmic reticulum (ER) stress response was the predominant event. Concomitant with transcriptomic analysis using mRNA expression, microarrays show ER stress response in the AuNP-treated cells. The ER stress protein markers' expression assay unveiled AuNPs as an efficient cellular ER stress elicitor. Upon ER stress, cellular responses, including reactive oxygen species increase, mitochondrial cytochrome *c* release, and mitochondria damage, chronologically occurred in the AuNP-treated cells. Conclusively, this study demonstrates that AuNPs cause cell death through induction of unmanageable ER stress.

KEYWORDS: nanogold particles · proteomics · transcriptomics · systems biology · endoplasmic reticulum stress

cytotoxicity of the physically synthesized AuNPs using the molecular beam epitaxy technique has been studied. Concomitantly, these ligand-free AuNPs show a size-dependent toxicity in cells.¹⁴ Thus, it becomes apparent that the plain AuNPs but not the surface-modified ligands induce death signals in cells. Intriguingly, even though numerous studies have shown the cytotoxicity

* Address correspondence to
056489@mail.fju.edu.tw.

Received for review November 2, 2010
and accepted November 8, 2011.

Published online November 22, 2011
10.1021/nn2027775

© 2011 American Chemical Society

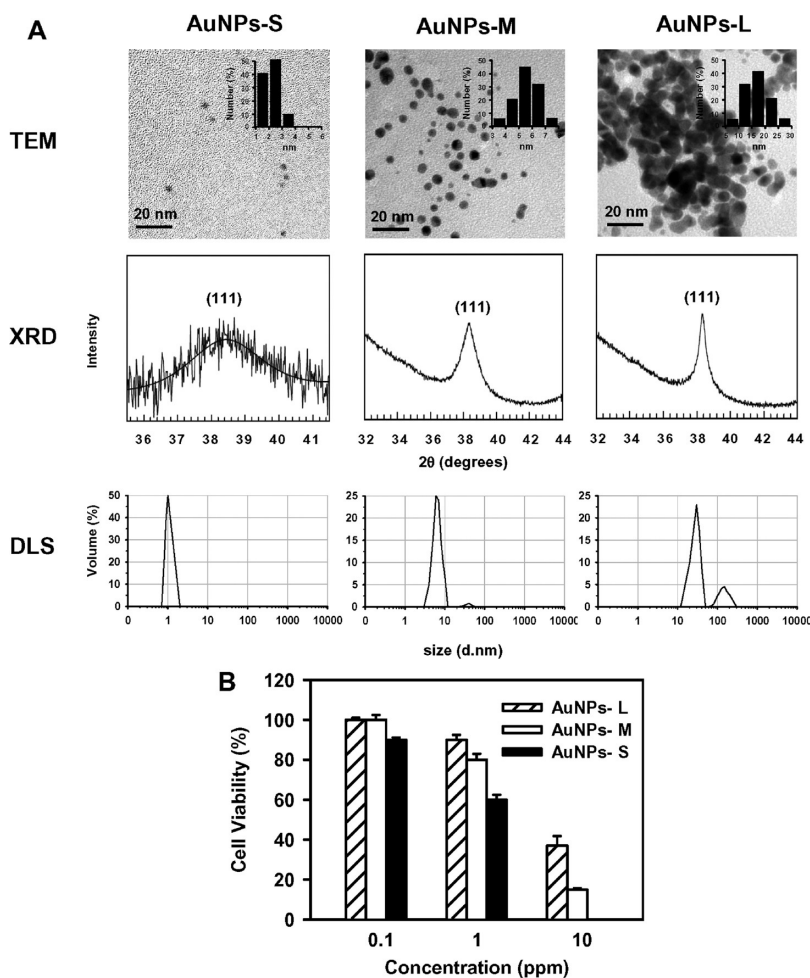


Figure 1. Characterization of the sizes and toxicity of different AuNPs. (A) Examples of TEM images, XRD spectra, and DLS profiles of three tested AuNPs including small AuNPs (AuNPs-S), medium AuNPs (AuNPs-M), and large AuNPs (AuNPs-L). Insets in the TEM images show the distribution of AuNPs. (B) Viability of K562 cells cultured 48 h in the media containing different AuNPs from 0.1 to 10 ppm.

TABLE 1. Size Distribution of Three Kinds of AuNPs Estimated by TEM, XRD, and DLS

	size distribution (nm)		
	TEM	XRD	DLS
AuNPs-S	mean (range) 2.2 (1–3)	mean/SD ^a 3.5/0.1	mean/SD (vol %) 1.0/0.1 (99%)
AuNPs-M	5.9 (5–6)	6.7/0.3	6.4/1.4 (97%)
AuNPs-L	17.0 (15–20)	14.3/0.8	29.1/5.4 (71.3%) 149.4/53.6 (28.7%)

^a SD: standard deviation.

of AuNPs *in vitro* and *in vivo*, the cellular mechanism underlying AuNP-induced toxicity remains elusive.

Proteomics is a fast growing discipline, which analyzes the expression and function of the whole gene products, namely, the proteome, within an organism. High-resolution protein separation and identification techniques, such as two-dimensional electrophoresis (2-DE) and mass spectrometry (MS), are widely utilized

in proteomic research.^{15–18} In addition, protein microarray is considered as another powerful tool for proteomic research.^{19,20} Incorporating probes (*e.g.*, antibodies) recognizing the protein of interest and protein microarrays (*e.g.*, antibody microarray) allows a high-throughput identification of expression and/or post-translational modification of proteins in one single experimental procedure.^{21,22} Nowadays, the above proteomic approaches have been demonstrated as useful tools for exploring cellular mechanisms.^{23,24}

Systems biology is an interdisciplinary subject that focuses on the systematic study of complex interactions in biological systems, using a perspective holism instead of reductionism to study them.^{25,26} Compared to most scientific methods used primarily toward reductionism, one of the goals of systems biology is to discover new emergent properties arising from the systemic view used by this discipline in order to understand the entirety of processes undergoing in a biological system. The investigations of systems biology require large-scale perturbation methods,

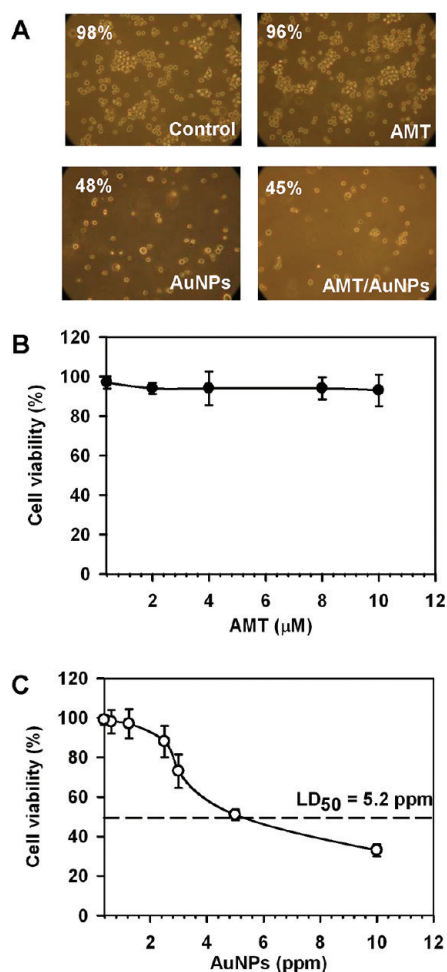


Figure 2. Comparison of the growth and viability for the AMT and AuNP-treated K562 cells. (A) Morphology of K562 cells ($40\times$ microscopic enlargement) cultured 48 h in the regular medium (top left panel) and the medium contain containing $0.4 \mu\text{M}$ AMT (top right panel), 5 ppm AuNPs (down left panel) or $0.4 \mu\text{M}$ AMT, 5 ppm AuNPs (bottom right panel). The viability of cells is indicated in the top left corner of each panel. The viability of K562 cultured under different concentrations of (B) AMT (closed circles) and (C) AuNPs (opened circles) was also examined. The half lethal dosage (LD_{50}) of AuNPs to K562 cells was indicated.

particularly the transcriptomic approaches using oligonucleotide microarrays.^{27,28} Data obtained using proteomic approaches, such as 2-DE, MS, and protein microarrays, can also be interpreted using systems biology analysis.^{29,30}

In this study, different omic approaches were used to identify the differentially expressed proteins/genes and phosphorylated proteins in the human leukemia K562 cells treated with AuNPs synthesized by the molecular beam epitaxy process. Systems biology analysis was employed alongside to systematically analyze the omic data for exploring the AuNP-elicted cellular mechanisms. It is found that AuNPs elicit endoplasmic reticulum (ER) stress responses in K562 cells. Unmanageable ER stress induced by AuNPs may result in cell death.

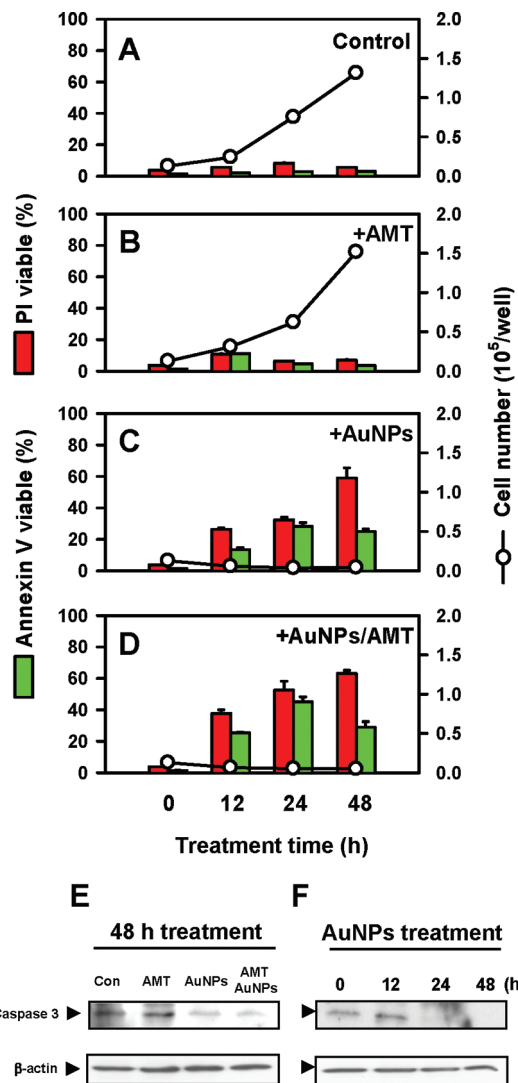


Figure 3. Growth inhibition and cell death phenomena in the AuNP-treated K562 cells. The growth curve (solid lines) and the ratio of propidium iodine (red bars) and annexin V (green bars) viable cells in the 0, 12, 24, and 48 h cultured cells. Treatment condition: (A) control; (B) $0.4 \mu\text{M}$ AMT; (C) 5 ppm AuNPs; (D) $0.4 \mu\text{M}$ AMT and 5 ppm AuNPs. (E) Expression of intact caspase 3 in the 48 h cultured K562 cells with different treatment. (F) Expression of intact caspase 3 of the 0, 12, 24, and 48 h AuNP-treated K562 cells. β -Actin was used as a loading control.

RESULTS

Size Characterization of AuNPs. Size distribution of three kinds of AuNPs with different diameters was initially examined using three different techniques (Figure 1A and Table 1). Transmission electron microscopy (TEM) analysis revealed the major diameter ranges of three kinds of AuNPs as 1–3 nm (small AuNPs, AuNPs-S), 5–6 nm (medium AuNPs, AuNPs-M), and 15–20 nm (large AuNPs, AuNPs-L). X-ray diffraction (XRD) analysis showed the diameter ranges of three kinds of AuNPs as 3.5 ± 0.1 nm (AuNPs-S), 6.7 ± 0.3 nm (AuNPs-M), and 14.3 ± 0.8 nm (AuNPs-L). Analyzed by dynamic light scattering (DLS), the diameter ranges of three kinds of AuNPs were 1.0 ± 0.1 nm (AuNPs-S), 6.4 ± 1.4 nm

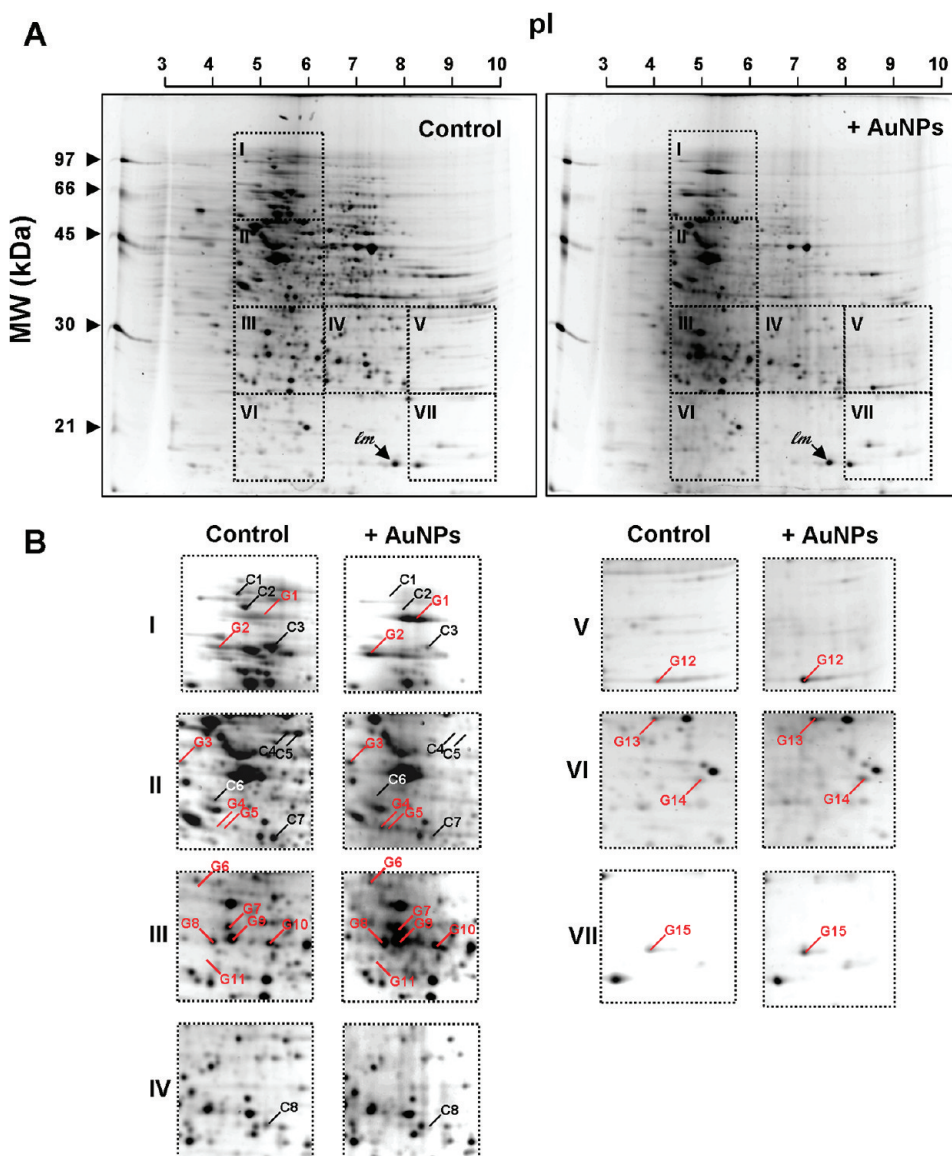


Figure 4. 2-DE analysis of the differentially expressed proteomes in the AuNP-treated K562 cells. (A) 2-DE gel images of intracellular proteomes of the untreated control (control) and the AuNP-treated K562 cells (+AuNPs). Seven image section pairs (I–VII) were cropped and enlarged. (B) Two-fold enlarged images of the cropped image sections in panel A. Up-regulated proteins in the untreated control and the AuNP-treated cells are indicated as C1–C8 and G1–G15, respectively; lm indicates the constitutively expressed protein selected as the landmark for image normalization.

(AuNPs-M), and 29.1 ± 5.4 (71%) and 149.4 ± 53.6 (29%) nm (AuNPs-L). Difference of size estimation occurs among the three techniques, probably because the analyzed samples were in different states (dry crystal form and liquid form). As suggested by the DLS technique that reveals the distribution of particles in liquid, AuNPs-S and AuNPs-M may comprise a higher homogeneity than AuNPs-L.

Determination of the Cytotoxicity of AuNPs. The cytotoxicities of AuNPs-S, AuNPs-M, and AuNPs-L were investigated using human chronic myelogenous leukemia K562 cells. Three kinds of AuNPs caused different degrees of cytotoxicity in K562 cells in a dose-dependent manner (Figure 1B). AuNPs-S showed more evident cytotoxicity than AuNPs-M and AuNPs-L. Considering the safety issue

that AuNPs-S are too toxic to cells, AuNPs-M (denoted as AuNPs afterward) were used for subsequent studies.

Interestingly, AuNPs more effectively inhibited growth of K562 cells than the commonly used antifolate aminopterin (AMT). Compared with the untreated control (Figure 2A, top left panel), the AuNP-treated K562 cells exhibited a profound growth inhibition and cell death (Figure 2A, bottom left panel). However, AMT did not affect the growth of K562 cells (Figure 2A, top right panel). The combination of AuNPs and AMT treatment also bestowed an obvious growth inhibition and cell death in K562 cells (Figure 2A, bottom left panel). The half lethal dosage (LD_{50}) of AuNPs in K562 cells was determined as 5.2 ppm (Figure 2C). Instead, as high as 10 μM AMT treatment did not affect the viability of

TABLE 2. Identity and Expression of the Differentially Expressed Proteins in the AuNP-Treated K562 Cells^a

spot no.	accession no.	protein description	M _r /pI		no. of peptides		sequence coverage (%)	relative expression ratio
			observed	theoretical	MOWSE score	queried		
C1	gi 292160	heat shock protein 70	97.9/5.10	78.9/5.13	39	41	1	1
C2	gi 6005942	valosin-containing protein	89.7/5.17	89.3/5.14	554	54	14	18
C3-1	gi 292059	MTHSP75	70.5/5.54	73.7/5.97	978	97	28	36
C3-2	gi 62897075	heat shock 70 kDa protein 9B precursor variant		73.6/5.87	951		27	36
C3-3	gi 7331218	keratin 1		66.0/8.16	256		5	7
C4-1	gi 7331218	keratin 1	47.8/5.80	66.0/8.16	95	44	2	4
C4-2	gi 292059	MTHSP75		73.7/5.97	61		1	2
C4-3	gi 5031753	heterogeneous nuclear ribonucleoprotein H1		49.5/5.89	38		1	4
C5	gi 7331218	keratin 1	47.7/5.95	66.0/8.16	49	4	3	5
C6-1	gi 306875	C protein	39.3/4.91	31.9/5.10	286	40	5	14
C6-2	gi 193785255	unnamed protein product		32.3/4.99	271		5	14
C6-3	gi 28317	unnamed protein product		59.5/5.17	122		2	3
C6-4	gi 292059	MTHSP75		73.7/5.97	82		1	2
C6-5	gi 386854	type II keratin subunit protein		52.8/5.31	42		1	3
C7-1	gi 4506667	ribosomal protein P0	34.4/5.65	34.3/5.71	307	41	8	27
C7-2	gi 189054178	unnamed protein product		66.0/7.62	118		2	3
C8-1	gi 28317	unnamed protein product	26.0/7.27	59.5/5.71	228	85	4	8
C8-2	gi 189054178	unnamed protein product		66.0/7.62	155		4	7
C8-3	gi 4139784	chain A, canine Gdp-Ran Q69I mutant		57.9/8.04	84		3	11
G1-1	gi 306891	90 kDa heat shock protein	86.7/5.21	83.2/4.97	375	61	8	11
G1-2	gi 83318444	HSP90AA1 protein		68.3/5.11	314		8	12
G1-3	gi 189054178	unnamed protein product		66.0/7.62	118		4	6
G1-4	gi 1082886	TRAP-1		75.3/8.43	95		1	2
G2-1	gi 194388088	unnamed protein product	70.5/4.90	63.9/5.39	269	132	7	12
G2-2	gi 7331218	keratin 1		66.0/8.16	265		6	9
G2-3	gi 386785	heat shock protein		69.9/5.42	261		7	12
G2-4	gi 35222	unnamed protein product		70.8/5.67	123		3	4
G3-1	gi 340219	vimentin	42.9/4.47	53.7/5.03	339	126	7	17
G3-2	gi 189054178	unnamed protein product		66.0/7.62	210		5	7
G3-3	gi 28336	mutant β -actin		41.8/5.22	64		1	4
G3-4	gi 307141	lysozyme precursor (EC 3.2.1.17)		16.5/9.38	57		2	8
G3-5	gi 157835338	chain A, mutant human lysozymes		14.7/9.28	57		2	9
G3-6	gi 157835340	chain A, human lysozyme		14.7/9.28	57		2	9
G3-7	gi 113584	Ig α -1 chain C region		37.6/6.08	39		1	4
G4-1	gi 189054178	unnamed protein product	36.6/5.00	66.0/7.62	156	114	3	5
G4-2	gi 386785	heat shock protein		69.8/5.42	104		2	3
G5-1	gi 189054178	unnamed protein product	36.6/5.11	66.0/7.62	470	140	9	13
G5-2	gi 28317	unnamed protein product		59.5/5.17	200		4	7
G6-1	gi 189054178	unnamed protein product	31.9/4.82	66.0/7.62	364	133	6	11
G6-2	gi 6694937	nudix hydrolase NUDT5		24.2/4.74	156		2	12
G7	gi 7331218	keratin 1	28.3/5.10	66.0/8.16	127	114	2	3
G8	gi 188492	heat shock-induced protein	27.4/4.91	70.4/5.76	110	108	3	6
G9-1	gi 7331218	keratin 1	27.5/5.14	66.0/8.16	144	99	3	4
G9-2	gi 431422	ran/TC4 binding protein		23.6/5.15	87		2	9
G9-3	gi 5729877	heat shock 70 kDa protein 8 isoform 1		70.8/5.37	51		1	1
G11	gi 553734	putative protein	26.0/4.80	NA	33	62	1	NA
G12	gi 4505591	peroxiredoxin 1	24.2/8.41	22.1/8.27	183	57	6	39
G14	gi 349905	chain F, mutant recombinant human Cu, Zn superoxide dismutase	19.7/5.74	15.7/5.70	66	41	3	18

TABLE 2. Continued

G15	gi 5031635	cofilin 1 (nonmuscle)	18.5/8.48	18.5/8.22	220	55	7	31	2.00
Im	gi 2981743	chain A, secyA complexed with hagia 5 (pseudo-symmetric monomer)	16.7/7.61	17.8/7.82	251	47	9	33	1

^aThe identities and expression of individual protein targets were analyzed by MS and 2-D gel image analysis software as described in methods. The accession number (no.), protein description, observed and theoretical molecular weight (M_r), isoelectric point (pI), identification MOWSE score, and the number of queried and matched peptides in MS experiments, sequence coverage (%) of identified protein targets are shown. In response to AuNP treatment, the relative expression ratio (AuNPs/con) of C1–C8 and G1–G15 spots was obtained by normalizing to the expression of corresponding spot pairs in the untreated control. NA, not available.

TABLE 3. Possible protein networks in response to AuNPs treatment. The most significant protein networks and canonical pathways in response to AuNPs treatment by analyzing the differentially expressed protein targets listed in Table 2 using IPA. In each suggested protein network, the top three suggested categories associated with different biological functions, the corresponding *P* value, and the involved molecules are shown. In each suggested canonical pathway, the ratio of involved protein targets to the total molecules in the pathway is expressed as ratio (%). In response to AuNPs treatment, the expression trend of involved protein targets (indicated in bold) is expressed by upward or downward arrows for up- and down-regulation respectively

Network 1 (score = 49)			
top three categories	top functions in category	P value	involved molecules
cellular function and maintenance	endoplasmic reticulum stress response	2.33×10^{-9}	ATXN3, ↑HSP90AA1 , ↑HSP90AB1 , ↑HSPA6 , ↑HSPA1A , ↑HSPA1L , ↓VCP
cellular compromise	endoplasmic reticulum stress response of cells	4.42×10^{-9}	ATXN3, ↑HSP90AA1 , ↑HSP90AB1 , ↑HSPA6 , ↑HSPA1A , ↑HSPA1L
post-translational modification	folding of protein	1.11×10^{-7}	BAG4, BAG5, ↑HSP90AA1 , ↑HSP90AB1 , ↑HSPA8 , HSPBP1
Network 2 (score = 17)			
top three categories	top functions in category	P value	involved molecules
cell signaling	quantity of calcium	2.03×10^{-1}	ANGPT2, Ca^{2+} , EPOR, GH1, GNRH1, JAK3, ↑LYZ , MYC, prostaglandin E2, prostaglandin F2 α , ↑SOD1
molecular transport	quantity of reactive oxygen species	1.74×10^{-7}	Ca^{2+} , EPOR, IFNB1, MYC, ↑PRDX1 , prostaglandin F2 α
vitamin and mineral metabolism	flux of calcium	2.24×10^{-7}	ANGPT2, Ca^{2+} , EPOR, GH1, GNRH1, GRIN1, prostaglandin E2, ↑SOD1
Canonical Pathways			
top three pathway	ratio (%)	involved protein targets	
glucocorticoid receptor signaling	2.85	↑HSPA8 , ↓HSPA4 , ↑HSPA1L , ↑HSP90AB1 , ↑HSPA1A , ↓HSPA9 , ↑HSPA6 , ↑HSP90AA1	
Huntington's disease signaling	2.54	↑HSPA8 , ↓HSPA4 , ↑HSPA1L , ↑HSPA1A , ↓HSPA9 , ↑HSPA6	
NRF2-mediated oxidative stress response	2.16	↑SOD1 , ↑PRDX1 , ↑ACTB , ↓VCP	

K562 cells (Figure 2B). Because most K562 cells are generally susceptible to the AMT treatment at nanomolar range,³¹ the utilized K562 cells might have generated antifolate resistance.

Characterization of the AuNP-Induced Cell Death. A time course study was performed to investigate the AuNP-induced death. The apoptotic and necrotic phenotypes were examined for the AuNPs/AMT-treated K562 cells. The untreated control and the AMT-treated cells grew exponentially with a minimal level of necrotic and apoptotic phenotypes detected (Figure 3A,B). Results show that the AuNP treatment inhibited growth of K562 cells, whereas K562 cells were insensitive to AMT. A significant growth inhibition as well as necrotic and apoptotic phenotypes was observed in the 12 h AuNP-treated K562 cells (Figure 3C). An apparent cell death, which accounts for 30% of the annexin and 60% of the propidium iodine viable cells, was detected in the 48 h AuNP-treated K562 cells. The combined treatment with AuNPs and AMT resulted in a similar growth inhibition and cell death phenomena in K562 cell (Figure 3D).

The AuNP-induced apoptosis was further confirmed by examining the activation of caspase 3 (Figure 3E). Cleavage of intact caspase 3 was detected 24 h after AuNPs treatment (Figure 3F).

Analysis of the Differentially Expressed Proteins in Response to AuNP Treatment. Proteomic approaches using 2-DE and MS were employed to identify the differentially expressed proteomes in response to AuNP treatment. In comparison to the untreated control, a distinct change of intracellular proteome was detected in the AuNP-treated K562 cells (Figure 4A). Fifteen proteins were found up-regulated (indicated as G1–G15 in Figure 4B), while eight proteins were down-regulated in response to AuNP treatment (indicated as C1–C8 in Figure 4B). Aforementioned regulated protein targets were identified using MS analysis (Table 2). Results showed that several heat shock protein cognates were found differentially expressed in response to AuNP treatment. Presumably, AuNPs induce stress in K562 cells.

Systems biology analysis using the ingenuity pathway analysis (IPA) software was employed to interpret

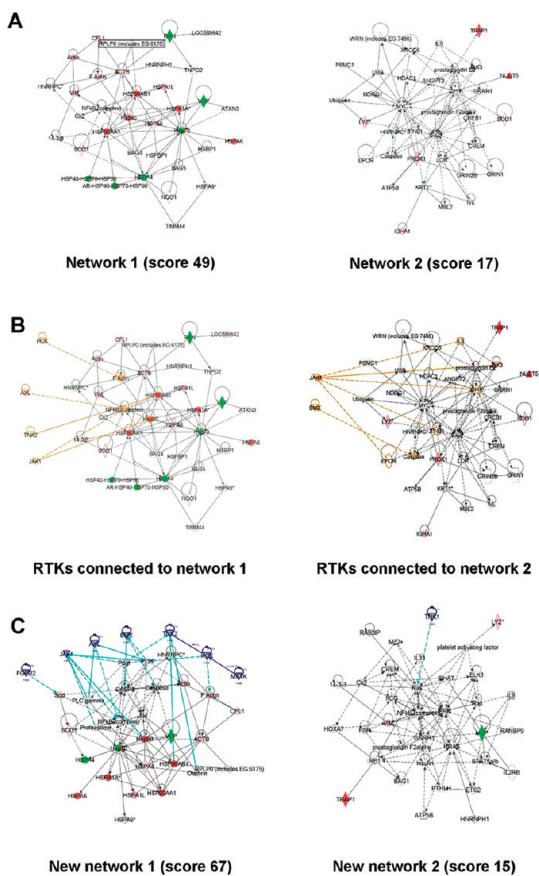


Figure 5. Protein networks in response to AuNP treatment. Protein networks suggested by IPA. (A) Most significant protein networks associated the differentially expressed proteome listed in Table 2. (B) Connection between the protein networks in panel A and differentially phosphorylated RTKs shown in Figure 6. RTKs and the corresponding connection are indicated by the orange color. (C) Most significant protein networks associated the differentially expressed proteome listed in Table 2 and differentially phosphorylated RTKs shown in Figure 6. RTKs and the corresponding connection are indicated by the blue color.

the biological significance of the above differentially expressed protein targets. Results of IPA revealed two most significant networks associated with different categories of distinct biological functions (Table 3). In network 1, the top three suggested categories are cellular function and maintenance, cellular compromise, and post-translational modification. These three categories closely relate to the functions of endoplasmic reticulum (ER) stress response and protein folding. In network 2, the top three suggested categories are cell signaling, molecular transport, and vitamin and mineral metabolism. The above categories closely relate to the functions of flux of calcium and quantity of reactive oxygen species (ROS). The protein interactions in network 1 and 2 are shown in Figure 5A.

Because protein folding is also the major event in response to ER stress,^{32–34} all suggested functions in network 1 relate to ER stress response. Additionally, as ER stress is reported to alter calcium homeostasis leading to ROS induction and apoptosis,^{34,35} all suggested

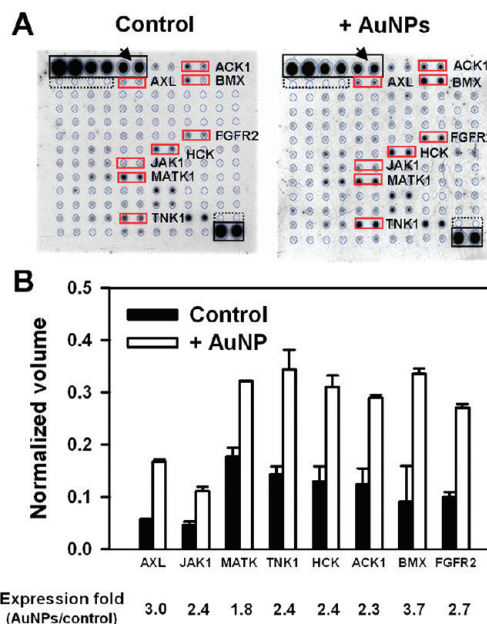


Figure 6. Protein microarray analysis of the differentially phosphorylated RTKs in the AuNP-treated K562 cells. (A) Hybridization results of RTK protein microarrays of the untreated control (control) and the AuNP-treated K562 cells (+AuNPs). Black and dashed squares indicate the positions of positive and negative controls, respectively. Red square indicates the position of differentially phosphorylated RTKs. (B) Phosphorylation level of the eight differentially phosphorylated RTK was quantitated by normalizing the image volume of individual spot to the one of positive control (arrows indicate). The expression fold of eight RTK in the AuNP-treated cells was obtained by normalizing to the corresponding spot pairs in the untreated control.

functions in network 2 relate to ER stress response, as well. The above results suggest the involvement of ER stress in response to AuNP treatment.

Analysis of the Differentially Phosphorylated Proteins in Response to AuNP Treatment. The phosphorylation status of protein receptor tyrosine kinase (RTK) was also examined in the AuNP-treated K562 cells using protein microarrays that simultaneously detect the phosphorylation level of 71 human RTK. It was found that the phosphorylation status of eight RTKs, including AXL, JAK1, MATK, TNK1, HCK, ACK1, BMX, and FGFR2, was upregulated in response to AuNP treatment (Figure 6A,B).

When employing the connect function of IPA to elucidate the relationship between the identified RTKs and networks 1 and 2, IPA, HCK, AXL, TNK 2, and JAK1 were linked to network 1; while JAK 1 and BMX belonged to network 2 (Figure 5B). Reperforming a new IPA analysis by simultaneously submitting the differentially phosphorylated RTKs and the differentially expressed proteins, eight RTKs targets were categorized into two new networks (Figure 5C). Notably, seven RTKs were allocated in the new network 1, which also highly associates with ER stress response (data not shown). The above results support the involvement of ER stress in response to AuNP treatment.

Analysis of the Differentially Expressed Genes in Response to AuNP Treatment. Transcriptomic approaches using human

TABLE 4. Possible Cellular Processes in Response to AuNP Treatment^a

GO database			
no.	cellular process	P value	differential expression ratio (\log_2)
			1.0 1.5 2.0
1	cellular macromolecule metabolic process	7.99 × 10 ⁻²¹	response to protein stimulus
2	negative regulation of biological process	6.19 × 10 ⁻¹⁹	transcription, DNA-dependent
3	negative regulation of cellular process	1.45 × 10 ⁻¹⁸	RNA biosynthetic process
4	macromolecule metabolic process	2.34 × 10 ⁻¹⁸	response to unfolded protein
5	response to protein stimulus	4.34 × 10 ⁻¹⁷	regulation of gene expression
6	metabolic process	5.92 × 10 ⁻¹⁷	RNA metabolic process
7	regulation of macromolecule metabolic process	4.25 × 10 ⁻¹⁶	regulation of cellular biosynthetic process
8	cellular metabolic process	5.06 × 10 ⁻¹⁶	regulation of macromolecule biosynthetic process
9	negative regulation of phosphate metabolic process	5.45 × 10 ⁻¹⁶	regulation of transcription
10	negative regulation of phosphorus metabolic process	5.45 × 10 ⁻¹⁶	transcription from RNA polymerase II promoter

GeneGo Database			
no.	cellular process	P value	differential expression ratio (\log_2)
			1.0 1.5 2.0
1	protein folding (response to unfolded proteins)	1.01 × 10 ⁻⁷	protein folding (response to unfolded proteins)
2	cell cycle G1-S (growth factor regulation)	5.63 × 10 ⁻⁶	protein folding (in normal condition)
3	cell cycle G1-S (interleukin regulation)	9.385 × 10 ⁻⁶	protein folding (in nucleus)
4	reproduction (FSH-β signaling pathway)	2.03 × 10 ⁻⁵	cell cycle G1-S (interleukin regulation)
5	protein folding (in normal condition)	4.60 × 10 ⁻⁵	apoptosis (endoplasmic reticulum stress pathway)
6	apoptosis (mitochondria)	6.32 × 10 ⁻⁵	cell cycle G1-S (growth factor regulation)
7	signal transduction (NOTCH signaling)	1.45 × 10 ⁻⁴	reproduction (FSH-beta signaling pathway)
8	inflammation (IL-6 signaling)	1.60 × 10 ⁻⁴	immune response (phagosome in antigen presentation)
9	reproduction (feeding and neurohormone signaling)	1.637 × 10 ⁻⁴	signal transduction (ERBB-family signaling)
10	development (hematopoiesis; erythropoietin pathway)	2.26 × 10 ⁻⁴	apoptosis (nucleus)

^a The most significant cellular processes suggested by analyzing the mRNA microarray data using the GeneGo software as described in methods. The differentially expressed genes with significance (*P* value <0.05) were analyzed against the gene ontology (GO) and GeneGo database with three expression criteria (differential expression ratio expressed as the value of \log_2). The top 10 suggested cellular processes were listed according to the *P* value. Cellular processes related to ER stress and apoptosis are shown in bold and underlined texts, respectively.

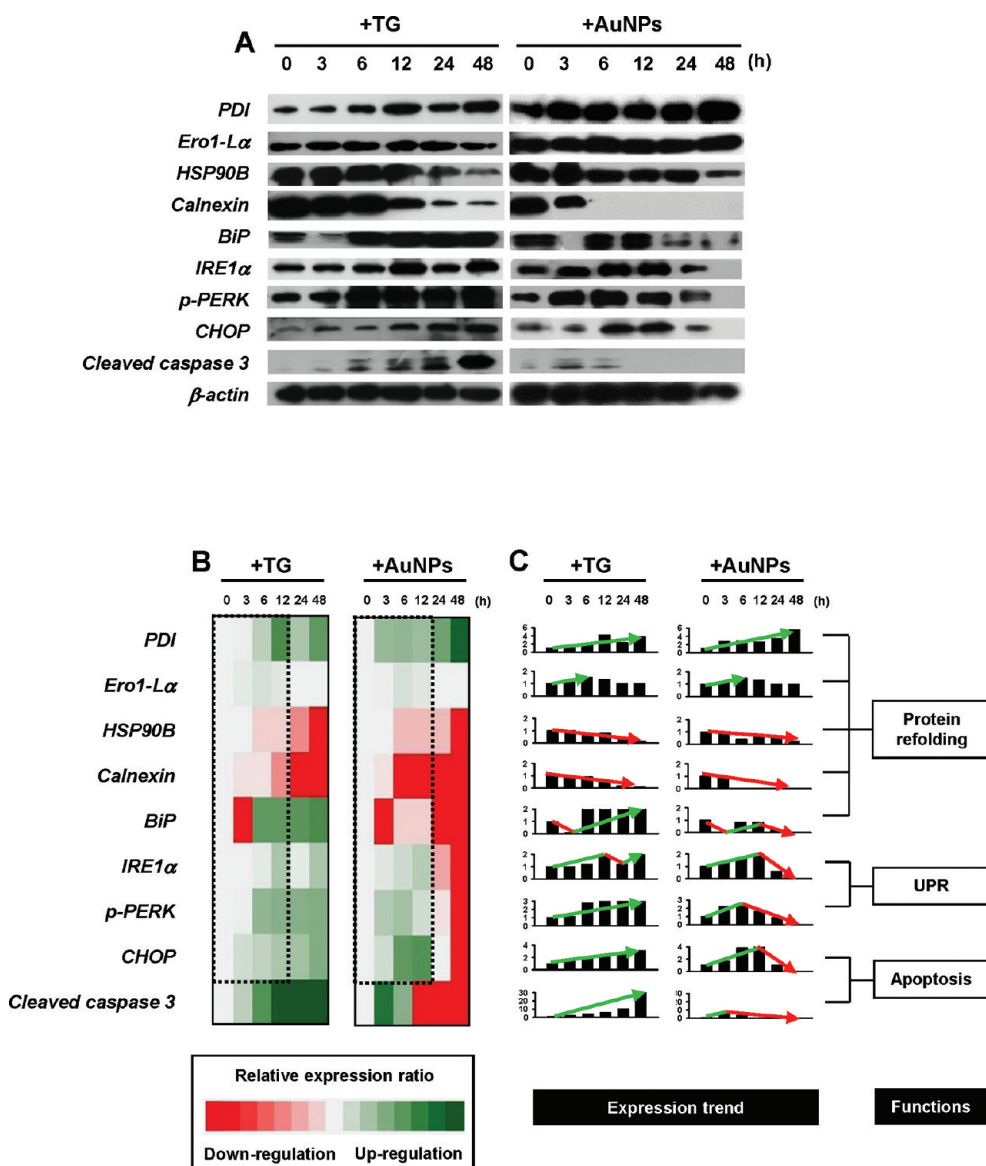


Figure 7. Expression of the ER stress marker proteins in the AuNP- and thapsigargin (TG)-treated K562 cells. (A) Expression of ER stress marker proteins, including PDI, Ero1-L α , HSP90B, calnexin, BiP, IRE1 α , the phosphorylated PERK (p-PERK), CHOP, cleaved caspase 3 in the 0, 3, 6, 12, 24, and 48 h thapsigargin (200 nM) and AuNP (5 ppm)-treated K562 cells were examined by immunostain. β -Actin was used as the loading control. (B) Expression profiles of ER stress and apoptotic marker proteins in the TG- and AuNP-treated K562 cells. The expression of proteins was quantitated as described in Methods. The relative expression ratio of individual marker protein was obtained by normalizing the expression to the untreated control (0 h treatment). A 15 scale heat map was used to compare the expression profile. Green and red squares indicate up- and down-regulation of proteins, respectively; white squares indicate consistent expression of proteins. Dashed line boxes highlight the expression of ER stress marker proteins in the 0 to 12 h treatment. (C) Expression trends of ER stress marker proteins in the TG- and AuNP-treated K562 cells. X-axis, treatment period (h); Y-axis, relative expression ratio of marker proteins. Green and red arrows indicate the trends of up- and down-regulation, respectively. The functions of marker proteins are also indicated.

mRNA microarrays were employed to identify the differentially expressed genes in the AuNP-treated K562 cells. Differentially expressed genes with significance were submitted for the analysis using another systems biology software, GeneGo. Two databases, the public gene ontology (GO) database and the commercial GeneGo database, were utilized to annotate the possible cellular processes in response to AuNP treatment.

As shown in Table 4, when employing a moderate criteria for gene data submission (differential expression where $\log_2 = 1.0$), annotations using the GO

database revealed response to protein stimulus as the fifth most significant cellular process. When employing a high stringent criteria for gene data submission (differential expression where $\log_2 = 1.5$ or 2.0), response to protein stimulus was identified as the most significant cellular process. Response to unfolded protein was also revealed by GO. On the other hand, annotations using the GeneGo database revealed protein folding response to unfolded proteins as the most significant cellular process, regardless of the submission criteria. Notably, mitochondria and ER-related

apoptosis was also suggested. The above results indicate that AuNPs may induce ER stress which may result in mitochondria and/or ER damages and also apoptosis of cells.

Expression of the ER Stress Marker in Response to AuNP treatment. Results from the above omics data and systems biology analysis pose the picture that AuNP treatment induces ER stress in K562 cells. Using a time course study, we further examined the expression of ER stress marker proteins, including PDI (protein disulfide isomerase), Ero1-L α (ER oxidase1-L α), HSP90B, calnexin, BiP (immunoglobulin binding protein), IRE1 α (inositol-requiring protein-1 α), p-PERK (phosphorylation of protein kinase RNA-like ER kinase), and CHOP (C/EBP homologous protein), in the AuNP-treated K562 cells. The expression of cleaved caspase 3 was also investigated. The treatment of standard ER stress inducer, thapsigargin (TG), was compared in parallel.

Either TG or AuNPs induced differential expression of ER stress marker proteins in K562 cells (Figure 7A). Particularly, TG and AuNPs induced a similar expression profile of ER stress marker proteins at the early phase of treatment (Figure 7B, 0–12 h, dashed line boxed). Additionally, the data showed that AuNPs induced higher degree of apoptosis than that by TG in K562 cells. Prompt up-regulation of CHOP and cleaved caspase 3, the two ER-stress-mediated apoptotic signals, was only detected in the AuNP-treated cells (Figure 7A,B). Moreover, analyzing the expression trends of marker proteins, AuNPs but not TG treatment showed apparent down-regulation of BiP, IRE1 α , and p-PERK, the proteins responsible for self-rescuing under ER stress, at the late phase of treatment (Figure 7C, 12–48 h). The above results advocate AuNPs as a kind of ER stress inducer that elicits unmanageable ER stress and then apoptosis in cells.

Investigation of Other Cellular Responses Induced by AuNPs. Systems biology analysis of omic data also implied the involvement of calcium flux, ROS quantity, and mitochondria damage in response to AuNP treatment. We also performed a time course study to examine the level of cytosolic calcium, ROS, cytochrome *c* release, mitochondria damage, apoptosis, and necrosis in the AuNP-treated K562 cells. The TG treatment was investigated in parallel.

In K562 cells, cytosolic calcium, the hallmark of the TG-induced ER stress, was increased transiently in 6 h after TG treatment (Figure 8A). Alternatively, AuNP treatment did not alter the level of cytosolic calcium in K562 cells. It suggests that AuNPs and TG comprise different mechanisms inducing ER stress. Additionally, a significant increase in cellular ROS was observed in 12 h after AuNP or TG treatment (Figure 8B). Evident cytochrome *c* release from mitochondria to cytosol was observed in 12 h after AuNP or TG treatment (Figure 8C). Considerable mitochondria damage was then detected in 12 and 24 h after AuNP and TG

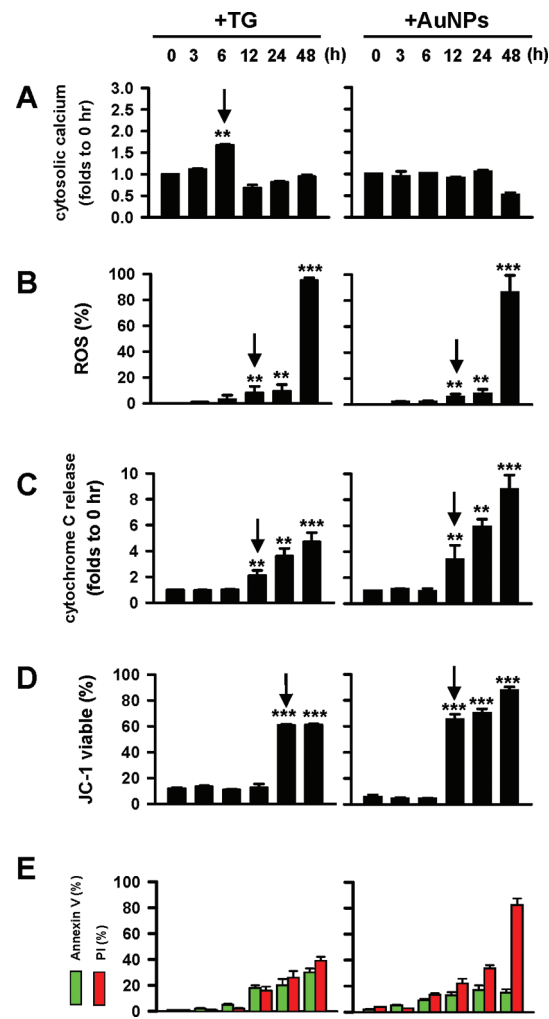


Figure 8. Time course study of cellular responses elicited by AuNP and TG treatment. Level of different cellular responses in the 0, 3, 6, 12, 24, and 48 h TG (200 nM) and AuNP (5 ppm)-treated K562 cells. (A) Cytosolic calcium. (B) ROS. (C) Cytochrome *c* release (cytosolic cytochrome *c*). (D) Mitochondria damage (JC-1 viable). (E) Apoptosis (Annexin V viable, green bars) and necrosis (PI viable, red bars). Data shown in panels A and C are expressed as expression folds normalized to the untreated control (0 h treatment). Data shown in panels B, D, and E are expressed as percentage individually normalized to total counted cells.

treatment, respectively (Figure 8D). Furthermore, both AuNPs and TG induced apoptosis as well as necrosis in K562 cells. More apoptotic phenotypes were detected in the early phase, while more necrotic phenotypes were found in the late phase of AuNP treatment (Figure 8E).

Considering that in K562 cells significant down-regulation of calnexin/BiP and up-regulation of p-PERK was detected in 3 h after AuNP treatment (Figure 7A,B), the time course study suggests that increase of ROS, cytochrome *c* release, and mitochondria damage are consequences of the AuNP-induced ER stress (see Discussion).

Cellular Interaction and Organelle Distribution of AuNPs. AuNPs may strongly interact with K562 cells. Significant

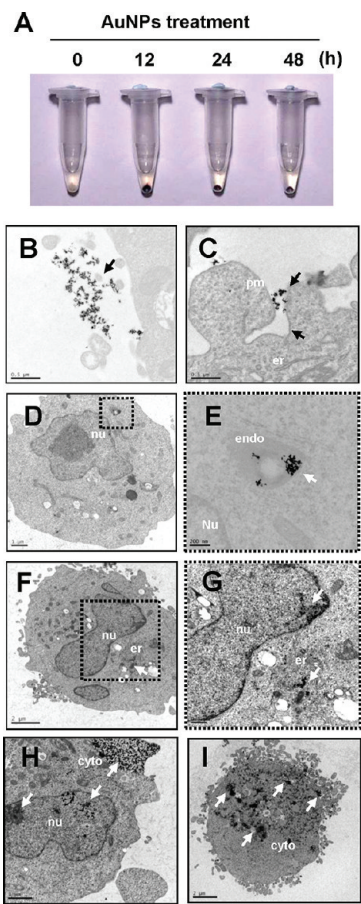


Figure 9. Cellular interaction and organelle distribution of AuNPs. (A) Visualization of the 0, 12, 24, and 48 h AuNP-treated K562 cells. The harvested cell pellets were extensively washed by PBS five times before photographing. (B–E) TEM images taken from the 3 h AuNP-treated cells; (F,G) TEM images taken from the 12 h AuNP-treated cells. (H,I) TEM images taken from the 24 h AuNP-treated cells. Panels E and G are the enlarged image sections of the dash line boxed areas in panels D and F, respectively. Arrows indicate the locations of AuNP clusters. Abbreviations used: pm, plasma membrane; nu, nucleus; endo, endosome; er, endoplasmic reticulum; cyto, cytosol.

retention of AuNPs was visually detected in the 12 h AuNP-treated cells (Figure 9A). Extensive washing by either phosphate buffer saline (PBS) or 10% SDS solution failed to detach AuNPs from the K562 cells after treatments (data not shown). Cellular interaction of AuNPs was further demonstrated using TEM. Clusters of AuNPs were found to associate with the plasma membrane (Figure 9B) or be endocytosed by K562 cells (Figure 9C).

Internalized AuNPs were detected in various organelles of K562 cells. At the early phase of treatment, AuNPs were generally found inside the single membrane organelles, presumably endosomes (Figure 9D,E). At the middle phase of treatment, AuNPs could be detected inside the nucleus or ER (Figure 9F,G). At the late phase of treatment, probably owing to the loss of membrane integrity, AuNPs were ubiquitously detected inside the cytoplasm of necrotic cells (Figure 9H,I).

DISCUSSION

In this study, a successful application of perspective holism to interpret the omic data was demonstrated. Using several omic approaches and systems biology analysis, ER stress responses were identified as one of the major cellular responses elicited by the physically synthesized AuNPs using the molecular beam epitaxy technique. Notably, IPA also indicated involvement of the canonical pathways, including glucocorticoid receptor signaling, Huntington's disease signaling, and NRF2-mediated oxidative stress response, with AuNP treatment (Table 3, IPA canonical pathways). Indeed, there is a close correlation between ER stress and the above-mentioned steroid signaling,³⁶ neurodegeneration,^{37,38} or NRF2-mediated signaling pathway.³⁹ As either the physically or the chemically synthesized AuNPs induced ER stress responses in different cell lines such as human chronic myelogenous leukemia K562, human embryonic kidney cells, human lymphoma cells, and mouse myeloma cells (unpublished results), the involvement of ER stress responses under AuNP treatment is confirmed.

ER is the major signal transducing organelle that senses and responds to changes of the homeostasis. ER stress is a well-studied cellular event with diverse signaling pathways (Supporting Information Figure 1).^{32–34} In the lumen of ER, unfolded proteins may cause stress response and subsequently induce self-rescuing or destruction responses in cells. There are three major responses to ER stress, including ER associated degradation (ERAD), unfolded protein response (UPR), and apoptosis.^{32,34} ERAD is generally regarded as a self-rescuing response by which misfolded proteins are removed from the ER into the cytoplasm where they are degraded by the ubiquitin proteasome system. Recently, the lysosome-dependent ERAD was also suggested.⁴⁰ When unfolded proteins accumulate in the ER, the resident chaperones such as BiP engage for protein folding, leading to a release of transmembrane proteins PERK, ATF6 (activating transcription factor-6), and IRE1 (inositol-requiring protein-1) responsible for the UPR. Depending on the elicited signaling pathway, UPR can be a self-rescuing or destruction response. For example, the PERK-mediated signaling pathway can either benefit cell survival through autophagy⁴¹ or cause apoptosis in cells via the translational up-regulation of ATF4/CHOP.^{42,43} The IRE1 α - and ATF6-mediated signaling pathways are reported to rescue cells through XBP1 (X-box binding protein-1)-dependent transcriptional up-regulation of some ER chaperones and foldases for protein refolding.^{44–46} The IRE1 β -mediated signaling pathway turns on apoptosis intervening by the cleavage of 28s rRNA.⁴⁷ In ER stress, ERAD or the self-rescuing UPR signaling pathway is regarded as a means to prevent from adopting the worst scenario, cell death. If ER stress persists for a certain

period, the caspase-dependent apoptosis is generally triggered with a result in cell death.³³ Recently, the ER stress-induced necrosis has also been reported.^{48,49}

It has been reported that AuNPs induce a prompt expression of pro-inflammatory genes in cells. For example, up-regulation of IL-1, IL-6, and TNF- α is detected in the 2 h AuNP-treated macrophages.¹⁴ In the present study, prompt up-regulation or down-regulation of ER stress marker proteins was detected in the AuNP-treated K562 cells (Figure 5). Up-regulation of PDI and Ero1-L α suggests the activation of IRE1 α - and ATF6-mediated self-rescuing response.^{44–46} Prompt down-regulation of calnexin, HSP90B (also known as GRP94), and BiP (also known as GRP78) indicates the rapid consumption of ER chaperones, which refold the misfolded proteins or direct their destruction through ERAD.^{32,34} A transient protein ubiquitination was only observed in the 6 h AuNP-treated K562 cells (data not shown). A consistent down-regulation of calnexin is considered as an antiapoptotic signaling because calnexin regulates ER-stress-mediated apoptosis in a chaperone function independent manner.^{50,51} Up-regulation of BiP in 6 h after AuNP treatment also suggests the activation of IRE1 α - and ATF6-mediated self-rescuing response.^{44–46} Nevertheless, down-regulation of the ER chaperones, HSP90B and BiP, indicates that the whole protein refolding responses were insufficient in the prolonged AuNP-treated cells. To relieve AuNP-induced ER stress, the PERK-mediated response, up-regulation of p-PERK, was also transiently activated. Additionally, several ER stress responsive genes with the binding site of XBP-1 in the promoter⁵² were found up-regulated in the mRNA microarray experiments (Supporting Information Table 1). Nevertheless, the above-mentioned self-rescuing responses in ER stress seems to be insufficient to rescue the AuNP-treated K562 cells, resulting in up-regulation of CHOP and cleaved caspase 3, as well as apoptotic and necrotic phenotypes. For the first time, a time course inspection of ER stress responses in the AuNP-treated cells was demonstrated in this study.

It is worthwhile to note that gold compounds can induce cellular responses other than ER stress. An *in vitro* antitumor effect of gold salts is associated with antimitochondrial activity and induced cell apoptosis, and thioredoxin reductase is suggested to be attributable to the effect.^{53–55} Our results show that AuNPs exert similar effects. IPA suggested alteration of the calcium homeostasis and induction of ROS in the AuNP-treated K562 cells (Table 3). GeneGo suggested mitochondria and ER-related apoptosis (Table 4). In the time course study of AuNP treatments, because apparent ER stress was detected at the early stage of treatment (Figure 7) while significant increase of ROS and cytosolic cytochrome c followed by mitochondria damage was detected at the middle or late stage of treatment (Figure 8), it is likely that the AuNP-induced ER stress may confer unfolded protein stress that

subsequently elicited ROS in cells. ROS may be scavenged by cytochrome c released from mitochondria. Overfluxing of cytochrome c by the persistent ER stress may induce mitochondria damage and thus apoptosis/necrosis in the long-time AuNP-treated cells. Coincidentally, ER stress has also been reported to alter calcium homeostasis leading to induction of ROS and subsequent apoptosis.^{34,35} The possible interaction between ER stress and other cellular responses was illustrated (Supporting Information Figure 2).

Notably, the apparent cytotoxicity and cellular responses induced by AuNPs varied among different groups.^{6,12,13} For example, Khan *et al.* have reported that 2 nM of the 18 nm citrated-coated AuNPs induced neither cell death nor ER stress in the human cervical cancer HeLa cells.⁵⁶ As shown in Supporting Information Table 2, when considering the atomic radius of Au as 144 pm, the dosage of AuNPs by Khan *et al.* is equivalent to 100 ppm. Therefore, the utilized ligand-free AuNPs demonstrated a higher cytotoxicity than some chemically synthesized AuNPs (Figure 1B). Indeed, it has been reported that the conjugated ligands on the chemically synthesized AuNPs may affect the cytotoxicity of AuNPs.^{57–60} Ligand-free AuNPs examined in present study were harvested in distilled water from a molecular beam epitaxy process; therefore, the detected cytotoxicity and the elicited cellular mechanisms should be considered as plain AuNPs.

The cellular interaction and uptake of AuNPs is another topic of interest in nanomedicines. AuNPs had been identified colocalizing with ER and Golgi apparatus in cells.⁶¹ Similar observation was made in this study (Figure 9F,G). The ER-mediated phagocytosis has been identified as a new mechanism by which macrophages take up pathogens against infectious diseases.⁶² Fusion of the ER membrane with the macrophage plasmalemma, underneath phagocytic cups is a source of membrane for phagosome formation in macrophages.⁶³ Presumably, AuNP clusters resemble a microorganism and can be phagocytosed into ER of cells by the above scenario. On the other hand, the serum-protein-mediated endocytosis of AuNPs has also been proposed.^{14,60,64} A peptide–BSA–AuNPs endocytosis in HeLa and 3T3/NIH cells had also been observed.⁶⁵ In this scenario, the clathrin- and COPI-coated vesicles may mediate the plasma membrane/endosome/Golgi apparatus/ER transportation of AuNPs.^{66,67} However, results from our AuNP affinity chromatography experiment demonstrated that no apparent interaction between the AuNPs and bovine and human serum albumin; other serum proteins may tightly interact with AuNPs *in vitro* (unpublished results). Possible AuNP transportation is also illustrated in Supporting Information Figure 2.

Nevertheless, the toxicity of AuNPs in normal cells is always a concern in nanomedicines. The utilized AuNPs (AuNPs-M) had an insignificant toxicity to the

peripheral blood mononuclear cells (PBMCs), which can be regarded as the normal counterpart of K562 cells. As high as 10 ppm, the utilized AuNPs did not reduce the viability of the *in vitro* culture PBMCs (Supporting Information Figure 3). Furthermore, it was observed that the utilized AuNPs may not induce structural chromosome aberration in Chinese hamster ovary CHO-K1 cells and had no detectable acute toxicity (14 day test) and subacute toxicity (28 day test) in mice and rats, which had been daily fed with AuNPs at the dose level of 5 mg/kg (5 ppm). A potential use of the utilized AuNPs in nanomedicines could be expected.

Our results indicate that the AuNP-treated cells may die from unmanageable ER stress. Undoubtedly, there is always an interest of utilizing AuNPs for cancer therapy. On the other hand, given that ER stress has been implicated engaging in the major pathogenesis of various chronic diseases, including Alzheimer's disease, Parkinson's disease, amyotrophic lateral sclerosis, polyglutamine disease, prion disease, stroke, bipolar disease, heart disease, atherosclerosis, type 1 and 2 diabetes, cancers, and autoimmune disease,^{32–34} the present study also sheds light on using AuNPs to induce an adaptive ER stress response for controlling the progress of chronic diseases.

METHODS

Preparation of AuNPs. AuNPs purchased from Gold NanoTech Inc. (Taipei, Taiwan) were prepared by a molecular beam epitaxy process as previously described.¹⁴ Briefly, in a system of ultra high vacuum (10^{-8} Pa), gold was evaporated and slowly deposited as AuNPs in distilled water. The sizes of AuNPs were managed depending on the evaporation time and electric current used. The concentration of AuNPs was determined using the inductively coupled plasma mass spectrometer (ICP-MS, PE-SCIEX ELAN 6100 DRC, Waltham, MA, USA).

Size Measurement of AuNPs. Particle sizes of AuNPs were analyzed using the transmission electron microscopy (TEM), the X-ray diffraction (XRD), and the dynamic light scattering (DLS) techniques. For TEM experiments, the JEM-1400 (JEOL, Japan) was operated at 110 kV. For XRD experiments, the MultiFlex X-ray diffractometer (Rigaku, Japan) with Cu $\text{K}\alpha_1$ ($\lambda = 0.15406$ nm) and Cu $\text{K}\alpha_2$ ($\lambda = 0.15444$ nm) radiations was used. To investigate the particle sizes of AuNPs, a AuNP solution was spread on a glass plate and then dried at room temperature before the XRD scan. Particle sizes of AuNPs were estimated using full width at half-maximum (fwhm) of the major XRD reflection signals (111) with Scherrer's equation

$$D = \frac{0.9\lambda}{\beta \cos \theta}$$

where D is the particle size, λ is the X-ray radiation wavelength, θ is the angle of XRD peak, and β (in radians) is the fwhm of the XRD peak. Values θ and β were determined using the PeakFit software (Systat, San Jose, CA) with the sum of Gaussian and Lorentzian profiles to fit the XRD peaks. Scherrer's equation has often been used to determine the mean (or average) sizes of nanoparticles by fitting the fwhm of the major XRD reflection peak.^{68,69} The corresponding results were found to be consistent with TEM technique.⁶⁹ For DLS experiments, the Malvern Zetasizer Nano S90 (Worcestershire, United Kingdom) was used.

Cell Culture and Viability Assays. Human chronic myelogenous leukemia K562 cells were cultured in the DMEM (Invitrogen, Grand Island, NY) based media containing 4 mM L-glutamine, 1 mM sodium pyruvate, 1% penicillin/streptomycin, and 10% fetal calf serum (FCS, PAA Laboratories, Pasching, Austria) at 37 °C with 5% CO₂ supplied. Cells were treated by AuNPs or/and aminopterin (AMT, Sigma, St. Louis, MO) at various concentrations as indicated. The growth of cells was examined by counting in 6-well cultures. The cell viability was examined using Trypan blue stain to exclude the dead cells and normalized the number of living cells to the total counted cells. The apparent half lethal dosages (LD₅₀) of AuNPs and AMT to K562 cells were measured as follows. Cells were initially treated by various concentrations of AuNPs or AMT for 2 days and measured for the cell viability as described above. After plotting the viability of treated cells against the corresponding concentration of treatment, the LD₅₀ of AuNPs and AMT to cells was then obtained using the nonlinear regression algorithm. The necrosis

and apoptosis of AuNP-treated cells was examined using the annexin V-FITC apoptosis detection kit (Strong Biotech Corp., Taipei, Taiwan) to microscopically count the annexin V and propidium iodine viable cells. All experiments were performed in triplicate to calculate the experimental averages and standard deviations.

2-DE Experiments. 2-DE was performed as reported previously with minor modification.⁷⁰ Briefly, trichloroacetic acid (TCA)-precipitated proteins from the 48 h AuNP-treated K562 cells and the control were dissolved into the standard 2-DE rehydration buffers containing 8 M urea, 2% 3-[3-cholamidopropyl]-dimethylammonio]-1-propanesulfonate (CHAPS), 0.5% IPG buffer, and 18 mM dithiothreitol (DTT). Protein samples (200 µg) were applied to IPG strips (13 cm, pH 3–10, linear range, GE Healthcare, Piscataway, NJ) using a rehydration loading method. The optimal IEF program was calculated using the IEF optimizer (Visual Protein, Taipei, Taiwan) as follows. After 12 h of rehydration, IEF was performed using 500 V for 1 h; 1000 V for 1 h; linearly ramping to 8000 V for 1 h, and finally 8000 V for 2.5 h on the IPGphor II system (GE Healthcare). The second dimensional electrophoresis was performed using 12.5% SDS-PAGE in the SE-600 electrophoresis system (GE Healthcare) at 40 mA constant current per gel after the strip equilibration procedure. All 2-D gels were stained by Sypro ruby protein stain (Invitrogen), and the 2-D gel images were documented using a xenon arc lamp-based CCD camera system (ProXPRESS, Perkin-Elmer, Waltham, MA, USA) with excitation/emission wavelength at 488 and 610 nm, respectively. The documented 2-D gel images were analyzed by Phoretix 2D Elite software (Nonlinear, Durham, NC). The expression of a protein spot target was calculated by normalizing the image volume to the corresponding one of landmark protein spot (Im) in individual 2-D gel image.

MS Protein Identifications. MS sample preparation was performed as reported previously.⁷⁰ Briefly, after restaining the Sypro ruby stained gels by VisPro 5 min protein stain kit (Visual Protein), protein targets on 2-D gels were manually excised at approximately 1 mm in diameter and processed according to the standard MS sample preparation protocol.⁷¹ In-gel digestion of the excised protein gel spots was carried out using MS-grade trypsin gold (Promega, Madison, WI, USA) overnight at 37 °C. Tryptic digests were extracted using 10 µL of Milli-Q water initially, followed by two extractions with a total of 20 µL of 0.1% trifluoroacetic acid (TFA). The combined extracts were dried in a vacuum concentrator at room temperature, and then dissolved in 1 µL of 5% acetonitrile with 0.5% TFA. The prepared MS samples were analyzed by ESI-QUAD-ToF MS analyzer (Q-TOF 2, Waters, Milford, MA). For each analyzed sample, all peak lists were generated for raw MS data using Masslynx (version 4.0 SP4) with signal-to-noise (S/N) threshold of 2. The processed data were analyzed using the MS/MS function in MASCOT searching engine (www.matrixscience.com). The search parameters were defined as follows: Database, NCBIInr (version: 20090619, 9111587 sequences; 3119984970 residues); Taxonomy, *Homo sapiens* (226 105 sequences); enzyme, trypsin;

variable modification, carbamidomethylation (cysteine) and oxidation (methionine); peptide tolerance, 0.2 Da; MS/MS tolerance, 0.2 Da; missed cleavage, one.

Protein Microarray. RayBio human RTK phosphorylation antibody array (RayBiotech, Inc., Norcross, GA) was used to examine the phosphorylation level of 71 human receptor tyrosine kinases in cells. All experimental procedures were performed according to manufacturer's protocol. The microarray data were quantitatively analyzed using TotalLab 100 software (Nonlinear).

mRNA Expression Microarray. Total RNA was extracted from cells using the RNeasy Mini kit (Qiagen, Valencia, CA, USA). The quality of RNA was assessed using Agilent 2100 Bioanalyzer (Agilent Technologies, Santa Clara, CA, USA). The Human Whole Genome OneArray v5 (Phalanx Biotech Group, Taiwan) contains 30 275 DNA oligonucleotide probes, and each probe is a 60-mer designed in the sense direction. Among the probes, 29 187 probes correspond to the annotated genes in RefSeq v38 and Ensembl v56 database.

Systems Biology Analysis. Systems biology analysis was performed using the Ingenuity Pathway Analysis software (IPA, Ingenuity Systems, www.ingenuity.com) and the MetaCore software v6.6 of GeneGo (<http://www.genego.com>). For IPA analysis, a data set containing gene identifiers and corresponding protein expression values from the 2-D gel image analysis was uploaded into the application. Each gene identifier was cross-examined for its corresponding gene object in the Ingenuity Pathways Knowledge Base (IPKB). These genes, called focus genes, were overlaid onto a global molecular network developed from information contained in IPKB. Networks of these focus genes were then algorithmically generated based on their connectivity. The functional analysis of a network identified the biological functions and/or diseases that were most significant to the genes in the network. Fisher's exact test was used to calculate a *P* value determining the probability that each biological function and/or disease assigned to that network is due to chance alone.

For GeneGo analysis, the differentially expressed genes with significance (*P* value <0.05), complete with the expression fold (\log_2 ratio), were uploaded from a Microsoft Excel worksheet onto the Metacore software. GeneGo recognizes the Gene Symbol identifiers and generates common cellular processes or molecular connections in response to AuNP treatment. The *P* values distribution of the Gene Ontology (GO) and GeneGo process network were analyzed.

Immunostain. Immunostain was used to evaluate apoptosis and ER stress responses related signals in cells as follows. Fifty micrograms of cell lysates was separated using 12.5% SDS-PAGE. Gels were then electro-blotted onto PVDF membranes and blocked using 5% skim milk in PBS. The locations of prestained protein markers on PVDF membranes were marked using Luminol Pen (Visual Protein) for subsequent chemiluminescent visualization. The blocked membranes were hybridized using primary antibody against intact caspase 3 (AP7563c, Abgent, San Diego, CA), cleaved caspase 3 (9662, Cell Signaling, Danvers, MA), ER stress marker proteins including PDI, Ero1-L α , BiP, calnexin, IRE1 α , phospho-PERK (Thr980), and CHOP (9956, ER stress antibody sampler kit, Cell Signaling), HSP90B (NB110-57066, Novus Biologicals, Littleton, CO), and β -actin (NB600-501, Novus Biologicals). After hybridizing with the HRP-conjugated horse anti-mouse (7076, Cell Signaling) or goat anti-rabbit secondary antibody (7074, Cell Signaling), the protein signals were developed using the VisGlow Plus chemiluminescent substrate (Visual Protein) by X-ray films. The image volume of protein signals was quantitated using TotalLab 100 software (Nonlinear). The expression of proteins was calculated by normalizing the image volume of individual protein bands to the one of β -actin in the same sample.

Assays of Cellular Responses. The AuNP-induced cellular responses were investigated as follows. The cytosolic calcium concentration was measured using the Fluo-3 a.m. method as previously described.⁷² The total ROS level was examined using the Image-iT LIVE Green reactive oxygen species detection kit (Invitrogen). The cytosolic cytochrome *c* level was examined using the cytochrome *c* releasing apoptosis assay kit (BioVision, Mountain View, CA). The disruption of the mitochondrial

transmembrane potential was examined using the MitoCapture mitochondrial apoptosis detection kit (BioVision). All experiments were performed in triplicate to calculate the experimental averages and standard deviations.

Acknowledgment. This work was supported by grants from Gold Nanotech, Inc., and Catholic Fu-Jen University (099630110 and 109931041001-2). The authors are most grateful and thank Dr. Chi-Feng Hung and Dr. Wen-Mein Wu in Fu Jen Catholic University for their valuable suggestions. We would also like to thank the Electron Microscope Laboratory, School of Medicine, Fu Jen Catholic University for all the technical assistance given in this study.

Supporting Information Available: Additional figures and tables. This material is available free of charge via the Internet at <http://pubs.acs.org>.

REFERENCES AND NOTES

- Mirkin, C. A.; Letsinger, R. L.; Mucic, R. C.; Storhoff, J. J. A DNA-Based Method for Rationally Assembling Nanoparticles into Macroscopic Materials. *Nature* **1996**, *382*, 607–609.
- Sokolov, K.; Follen, M.; Aaron, J.; Pavlova, I.; Malpica, A.; Lotan, R.; Richards-Kortum, R. Real-Time Vital Optical Imaging of Precancer Using Anti-Epidermal Growth Factor Receptor Antibodies Conjugated to Gold Nanoparticles. *Cancer Res.* **2003**, *63*, 1999–2004.
- Levy, R.; Thanh, N. T.; Doty, R. C.; Hussain, I.; Nichols, R. J.; Schiffrin, D. J.; Brust, M.; Fernig, D. G. Rational and Combinatorial Design of Peptide Capping Ligands for Gold Nanoparticles. *J. Am. Chem. Soc.* **2004**, *126*, 10076–10084.
- Shaw, I. C. Gold-Based Therapeutic Agents. *Chem. Rev.* **1999**, *99*, 2589–2600.
- Cuenca, A. G.; Jiang, H.; Hochwald, S. N.; Delano, M.; Cance, W. G.; Grobmyer, S. R. Emerging Implications of Nanotechnology on Cancer Diagnostics and Therapeutics. *Cancer* **2006**, *107*, 459–466.
- Boisselier, E.; Astruc, D. Gold Nanoparticles in Nanomedicine: Preparations, Imaging, Diagnostics, Therapies and Toxicity. *Chem. Soc. Rev.* **2009**, *38*, 1759–1782.
- Tsai, C. Y.; Shiao, A. L.; Chen, S. Y.; Chen, Y. H.; Cheng, P. C.; Chang, M. Y.; Chen, D. H.; Chou, C. H.; Wang, C. R.; Wu, C. L. Amelioration of Collagen-Induced Arthritis in Rats by Nanogold. *Arthritis Rheum.* **2007**, *56*, 544–554.
- LaRocque, J.; Bharali, D. J.; Mousa, S. A. Cancer Detection and Treatment: The Role of Nanomedicines. *Mol. Biotechnol.* **2009**, *42*, 358–366.
- Paciotti, G. F.; Myer, L.; Weinreich, D.; Goia, D.; Pavel, N.; McLaughlin, R. E.; Tamarkin, L. Colloidal Gold: A Novel Nanoparticle Vector for Tumor Directed Drug Delivery. *Drug Delivery* **2004**, *11*, 169–183.
- Huang, X. H.; Jain, P. K.; El-Sayed, I. H.; El-Sayed, M. A. Plasmonic Photothermal Therapy (Pptt) Using Gold Nanoparticles. *Laser Med. Sci.* **2008**, *23*, 217–228.
- Allison, R. R.; Mota, H. C.; Bagnato, V. S.; Sibata, C. H. Bio-Nanotechnology and Photodynamic Therapy - State of the Art Review. *Photodiagn. Photodyn.* **2008**, *5*, 19–28.
- Lewinski, N.; Colvin, V.; Drezek, R. Cytotoxicity of Nanoparticles. *Small* **2008**, *4*, 26–49.
- Murphy, C. J.; Gole, A. M.; Stone, J. W.; Sisco, P. N.; Alkilany, A. M.; Goldsmith, E. C.; Baxter, S. C. Gold Nanoparticles in Biology: Beyond Toxicity to Cellular Imaging. *Acc. Chem. Res.* **2008**, *41*, 1721–1730.
- Yen, H. J.; Hsu, S. H.; Tsai, C. L. Cytotoxicity and Immunological Response of Gold and Silver Nanoparticles of Different Sizes. *Small* **2009**, *5*, 1553–1561.
- Gorg, A.; Weiss, W.; Dunn, M. J. Current Two-Dimensional Electrophoresis Technology for Proteomics. *Proteomics* **2004**, *4*, 3665–3685.
- Rossignol, M.; Peltier, J. B.; Mock, H. P.; Matros, A.; Maldonado, A. M.; Jorrin, J. V. Plant Proteome Analysis: A 2004–2006 Update. *Proteomics* **2006**, *6*, 5529–5548.
- McGregor, E.; Dunn, M. J. Proteomics of the Heart: Unraveling Disease. *Circ. Res.* **2006**, *98*, 309–321.

18. Cash, P. Proteomics in the Study of the Molecular Taxonomy and Epidemiology of Bacterial Pathogens. *Electrophoresis* **2009**, *30*, S133–S141.
19. Haab, B. B. Advances in Protein Microarray Technology for Protein Expression and Interaction Profiling. *Curr. Opin. Drug Discovery Dev.* **2001**, *4*, 116–123.
20. MacBeath, G. Protein Microarrays and Proteomics. *Nat. Genet.* **2002**, *32*, 526–532.
21. Chen, S.; LaRoche, T.; Hamelinck, D.; Bergsma, D.; Brenner, D.; Simeone, D.; Brand, R. E.; Haab, B. B. Multiplexed Analysis of Glycan Variation on Native Proteins Captured by Antibody Microarrays. *Nat. Methods* **2007**, *4*, 437–444.
22. Acosta, J. C.; O'Loughlin, A.; Banito, A.; Guijarro, M. V.; Augert, A.; Raguz, S.; Fumagalli, M.; Da Costa, M.; Brown, C.; Popov, N.; et al. Chemokine Signaling via the Cxcr2 Receptor Reinforces Senescence. *Cell* **2008**, *133*, 1006–1018.
23. Antelmann, H.; Hecker, M.; Zuber, P. Proteomic Signatures Uncover Thiol-Specific Electrophile Resistance Mechanisms in *Bacillus subtilis*. *Expert Rev. Proteomics* **2008**, *5*, 77–90.
24. Radulovic, M.; Godovac-Zimmermann, J. Proteomic Approaches To Understanding the Role of the Cytoskeleton in Host-Defense Mechanisms. *Expert Rev. Proteomics* **2011**, *8*, 117–126.
25. Ideker, T.; Galitski, T.; Hood, L. A New Approach To Decoding Life: Systems Biology. *Annu. Rev. Genomics Hum. Genet.* **2001**, *2*, 343–372.
26. Sauer, U.; Heinemann, M.; Zamboni, N. Genetics. Getting Closer to the Whole Picture. *Science* **2007**, *316*, 550–551.
27. Benson, M.; Breitling, R. Network Theory To Understand Microarray Studies of Complex Diseases. *Curr. Mol. Med.* **2006**, *6*, 695–701.
28. Liu, E. T.; Kuznetsov, V. A.; Miller, L. D. In the Pursuit of Complexity: Systems Medicine in Cancer Biology. *Cancer Cell* **2006**, *9*, 245–247.
29. Han, C. L.; Chien, C. W.; Chen, W. C.; Chen, Y. R.; Wu, C. P.; Li, H.; Chen, Y. J. A Multiplexed Quantitative Strategy for Membrane Proteomics: Opportunities for Mining Therapeutic Targets for Autosomal Dominant Polycystic Kidney Disease. *Mol. Cell. Proteomics* **2008**, *7*, 1983–1997.
30. Dhungana, S.; Merrick, B. A.; Tomer, K. B.; Fessler, M. B. Quantitative Proteomics Analysis of Macrophage Rafts Reveals Compartmentalized Activation of the Proteasome and of Proteasome-Mediated Erk Activation in Response to Lipopolysaccharide. *Mol. Cell. Proteomics* **2009**, *8*, 201–213.
31. McGuire, J. J.; Russell, C. A.; Bolanowska, W. E.; Freitag, C. M.; Jones, C. S.; Kalman, T. I. Biochemical and Growth Inhibition Studies of Methotrexate and Aminopterin Analogues Containing a Tetrazole Ring in Place of the γ -Carboxyl Group. *Cancer Res.* **1990**, *50*, 1726–1731.
32. Xu, C.; Baily-Maitre, B.; Reed, J. C. Endoplasmic Reticulum Stress: Cell Life and Death Decisions. *J. Clin. Invest.* **2005**, *115*, 2656–2664.
33. Ron, D.; Walter, P. Signal Integration in the Endoplasmic Reticulum Unfolded Protein Response. *Nat. Rev. Mol. Cell. Biol.* **2007**, *8*, 519–529.
34. Kim, I.; Xu, W.; Reed, J. C. Cell Death and Endoplasmic Reticulum Stress: Disease Relevance and Therapeutic Opportunities. *Nat. Rev. Drug Discovery* **2008**, *7*, 1013–1030.
35. Kitamura, M. Endoplasmic Reticulum Stress and Unfolded Protein Response in Renal Pathophysiology: Janus Faces. *Am. J. Physiol. Renal Physiol.* **2008**, *295*, F323–334.
36. Rao, R. V.; Niazi, K.; Mollahan, P.; Mao, X.; Crippen, D.; Poksay, K. S.; Chen, S.; Bredesen, D. E. Coupling Endoplasmic Reticulum Stress to the Cell-Death Program: A Novel Hsp90-Independent Role for the Small Chaperone Protein P23. *Cell Death Dis.* **2006**, *13*, 415–425.
37. Lindholm, D.; Wootz, H.; Korhonen, L. Er Stress and Neurodegenerative Diseases. *Cell Death Dis.* **2006**, *13*, 385–392.
38. Wei, H.; Kim, S. J.; Zhang, Z.; Tsai, P. C.; Wisniewski, K. E.; Mukherjee, A. B. Er and Oxidative Stresses Are Common Mediators of Apoptosis in Both Neurodegenerative and Non-neurodegenerative Lysosomal Storage Disorders and Are Alleviated by Chemical Chaperones. *Hum. Mol. Genet.* **2008**, *17*, 469–477.
39. Cullinan, S. B.; Diehl, J. A. Coordination of Er and Oxidative Stress Signaling: The Perk/Nrf2 Signaling Pathway. *Int. J. Biochem. Cell Biol.* **2006**, *38*, 317–332.
40. Fujita, E.; Kouroku, Y.; Isoai, A.; Kumagai, H.; Misutani, A.; Matsuda, C.; Hayashi, Y. K.; Momoi, T. Two Endoplasmic Reticulum-Associated Degradation (Erad) Systems for the Novel Variant of the Mutant Dysferlin: Ubiquitin/Proteasome Erad(l) and Autophagy/Lysosome Erad(l). *Hum. Mol. Genet.* **2007**, *16*, 618–629.
41. Kouroku, Y.; Fujita, E.; Tanida, I.; Ueno, T.; Isoai, A.; Kumagai, H.; Ogawa, S.; Kaufman, R. J.; Kominami, E.; Momoi, T. Er Stress (Perk/Eif2 α Phosphorylation) Mediates the Polyglutamine-Induced Lc3 Conversion, an Essential Step for Autophagy Formation. *Cell Death Dis.* **2007**, *14*, 230–239.
42. Oyadomari, S.; Mori, M. Roles of Chop/Gadd153 in Endoplasmic Reticulum Stress. *Cell Death Dis.* **2004**, *11*, 381–389.
43. Toth, A.; Nickson, P.; Mandl, A.; Bannister, M. L.; Toth, K.; Erhardt, P. Endoplasmic Reticulum Stress as a Novel Therapeutic Target in Heart Diseases. *Cardiovasc. Hematol. Disord. Drug Targets* **2007**, *7*, 205–218.
44. Yoshida, H.; Matsui, T.; Yamamoto, A.; Okada, T.; Mori, K. Xbp1Mrna Is Induced by Atf6 and Spliced by Ire1 in Response to Er Stress To Produce a Highly Active Transcription Factor. *Cell* **2001**, *107*, 881–891.
45. Baumeister, P.; Luo, S.; Skarnes, W. C.; Sui, G.; Seto, E.; Shi, Y.; Lee, A. S. Endoplasmic Reticulum Stress Induction of the Grp78/Bip Promoter: Activating Mechanisms Mediated by Yy1 and Its Interactive Chromatin Modifiers. *Mol. Cell. Biol.* **2005**, *25*, 4529–4540.
46. Yamamoto, K.; Sato, T.; Matsui, T.; Sato, M.; Okada, T.; Yoshida, H.; Harada, A.; Mori, K. Transcriptional Induction of Mammalian Er Quality Control Proteins Is Mediated by Single or Combined Action of Atf6 α and Xbp1. *Dev. Cell* **2007**, *13*, 365–376.
47. Iwawaki, T.; Hosoda, A.; Okuda, T.; Kamigori, Y.; Nomura-Furukawa, C.; Kimata, Y.; Tsuru, A.; Kohno, K. Translational Control by the Er Transmembrane Kinase/Ribonuclease Ire1 under Er Stress. *Nat. Cell Biol.* **2001**, *3*, 158–164.
48. Gills, J. J.; Lopiccolo, J.; Tsurutani, J.; Shoemaker, R. H.; Best, C. J.; Abu-Asab, M. S.; Borojerdi, J.; Warfel, N. A.; Gardner, E. R.; Danish, M.; et al. Nelfinavir, a Lead Hiv Protease Inhibitor, Is a Broad-Spectrum, Anticancer Agent That Induces Endoplasmic Reticulum Stress, Autophagy, and Apoptosis *In Vitro* and *In Vivo*. *Clin. Cancer Res.* **2007**, *13*, 5183–5194.
49. Ullman, E.; Fan, Y.; Stawowczyk, M.; Chen, H. M.; Yue, Z.; Zong, W. X. Autophagy Promotes Necrosis in Apoptosis-Deficient Cells in Response to Er Stress. *Cell Death Dis.* **2008**, *15*, 422–425.
50. Zuppini, A.; Groenendyk, J.; Cormack, L. A.; Shore, G.; Opas, M.; Bleackley, R. C.; Michalak, M. Calnexin Deficiency and Endoplasmic Reticulum Stress-Induced Apoptosis. *Biochemistry* **2002**, *41*, 2850–2858.
51. Delom, F.; Emadali, A.; Cocolakis, E.; Lebrun, J. J.; Nantel, A.; Chevet, E. Calnexin-Dependent Regulation of Tunicamycin-Induced Apoptosis in Breast Carcinoma Mcf-7 Cells. *Cell Death Dis.* **2007**, *14*, 586–596.
52. Szczesna-Skorupa, E.; Chen, C. D.; Liu, H.; Kemper, B. Gene Expression Changes Associated with the Endoplasmic Reticulum Stress Response Induced by Microsomal Cytochrome P450 Overproduction. *J. Biol. Chem.* **2004**, *279*, 13953–13961.
53. Gromer, S.; Arscott, L. D.; Williams, C. H., Jr.; Schirmer, R. H.; Becker, K. Human Placenta Thioredoxin Reductase. Isolation of the Selenoenzyme, Steady State Kinetics, and Inhibition by Therapeutic Gold Compounds. *J. Biol. Chem.* **1998**, *273*, 20096–20101.
54. McKeage, M. J.; Berners-Price, S. J.; Galettis, P.; Bowen, R. J.; Brouwer, W.; Ding, L.; Zhuang, L.; Baguley, B. C. Role of Lipophilicity in Determining Cellular Uptake and Antitumour

- Activity of Gold Phosphine Complexes. *Cancer Chemother. Pharmacol.* **2000**, *46*, 343–350.
55. Liu, J. J.; Galettis, P.; Farr, A.; Maharaj, L.; Samarasinha, H.; McGechan, A. C.; Baguley, B. C.; Bowen, R. J.; Berners-Price, S. J.; McKeage, M. J. *In Vitro* Antitumour and Hepatotoxicity Profiles of Au(I) and Ag(I) Bidentate Pyridyl Phosphine Complexes and Relationships to Cellular Uptake. *J. Inorg. Biochem.* **2008**, *102*, 303–310.
 56. Khan, J. A.; Pillai, B.; Das, T. K.; Singh, Y.; Maiti, S. Molecular Effects of Uptake of Gold Nanoparticles in HeLa Cells. *ChemBioChem* **2007**, *8*, 1237–1240.
 57. Goodman, C. M.; McCusker, C. D.; Yilmaz, T.; Rotello, V. M. Toxicity of Gold Nanoparticles Functionalized with Cationic and Anionic Side Chains. *Bioconjugate Chem.* **2004**, *15*, 897–900.
 58. Connor, E. E.; Mwamuka, J.; Gole, A.; Murphy, C. J.; Wyatt, M. D. Gold Nanoparticles Are Taken up by Human Cells but Do Not Cause Acute Cytotoxicity. *Small* **2005**, *1*, 325–327.
 59. Leonov, A. P.; Zheng, J. W.; Clogston, J. D.; Stern, S. T.; Patri, A. K.; Wei, A. Detoxification of Gold Nanorods by Treatment with Polystyrenesulfonate. *ACS Nano* **2008**, *2*, 2481–2488.
 60. Alkilany, A. M.; Nagaria, P. K.; Hexel, C. R.; Shaw, T. J.; Murphy, C. J.; Wyatt, M. D. Cellular Uptake and Cytotoxicity of Gold Nanorods: Molecular Origin of Cytotoxicity and Surface Effects. *Small* **2009**, *5*, 701–708.
 61. Chang, M. Y.; Shiau, A. L.; Chen, Y. H.; Chang, C. J.; Chen, H. H.; Wu, C. L. Increased Apoptotic Potential and Dose-Enhancing Effect of Gold Nanoparticles in Combination with Single-Dose Clinical Electron Beams on Tumor-Bearing Mice. *Cancer Sci.* **2008**, *99*, 1479–1484.
 62. Desjardins, M. ER-Mediated Phagocytosis: A New Membrane for New Functions. *Nat. Rev. Immunol.* **2003**, *3*, 280–291.
 63. Gagnon, E.; Duclos, S.; Rondeau, C.; Chevet, E.; Cameron, P. H.; Steele-Mortimer, O.; Paiement, J.; Bergeron, J. J.; Desjardins, M. Endoplasmic Reticulum-Mediated Phagocytosis Is a Mechanism of Entry into Macrophages. *Cell* **2002**, *110*, 119–131.
 64. Chithrani, D. B. Intracellular Uptake, Transport, and Processing of Gold Nanostructures. *Mol. Membr. Biol.* **2010**, *27*, 299–311.
 65. Tkachenko, A. G.; Xie, H.; Liu, Y.; Coleman, D.; Ryan, J.; Glomm, W. R.; Shipton, M. K.; Franzen, S.; Feldheim, D. L. Cellular Trajectories of Peptide-Modified Gold Particle Complexes: Comparison of Nuclear Localization Signals and Peptide Transduction Domains. *Bioconjugate Chem.* **2004**, *15*, 482–490.
 66. Kreis, T. E.; Lowe, M.; Pepperkok, R. Cops Regulating Membrane Traffic. *Annu. Rev. Cell. Dev. Biol.* **1995**, *11*, 677–706.
 67. Gorelick, F. S.; Shugrue, C. Exiting the Endoplasmic Reticulum. *Mol. Cell. Endocrinol.* **2001**, *177*, 13–18.
 68. Patterson, L. The Scherrer Formula for X-ray Particle Size Determination. *Phys. Rev.* **1939**, *56*, 978–982.
 69. Tang, Z. X.; Sorensen, C. M.; Klabunde, K. J.; Hadjipanayis, G. C. Size-Dependent Curie-Temperature in Nanoscale MnFe₂O₄ Particles. *Phys. Rev. Lett.* **1991**, *67*, 3602–3605.
 70. Lin, C. Y.; Wang, V.; Shui, H. A.; Juang, R. H.; Hour, A. L.; Chen, P. S.; Huang, H. M.; Wu, S. Y.; Lee, J. C.; Tsai, T. L.; et al. A Comprehensive Evaluation of Imidazole-Zinc Reverse Stain for Current Proteomic Researches. *Proteomics* **2009**, *9*, 696–709.
 71. Simpson, R. J. *Quantifying Protein by Bicinchoninic Acid*; Cold Spring Harbor Laboratory Press: New York, 2003; pp 846–847.
 72. Minta, A.; Kao, J. P.; Tsien, R. Y. Fluorescent Indicators for Cytosolic Calcium Based on Rhodamine and Fluorescein Chromophores. *J. Biol. Chem.* **1989**, *264*, 8171–8178.